01 Jan 2016

Role of Composition and Structure on the Properties of Metal/Multifunctional Ceramic Interfaces

Fang Yin Lin

Aleksandr V. Chernatynskiy
Missouri University of Science and Technology, aleksandrc@mst.edu

Juan Claudio Nino

Jacob L. Jones

et. al. For a complete list of authors, see https://scholarsmine.mst.edu/phys_facwork/490

Recommended Citation

F. Y. Lin et al., "Role of Composition and Structure on the Properties of Metal/Multifunctional Ceramic Interfaces," *Journal of Applied Physics*, vol. 120, no. 4, American Institute of Physics (AIP), Jan 2016. The definitive version is available at https://doi.org/10.1063/1.4959074

Role of composition and structure on the properties of metal/multifunctional ceramic interfaces

Fang-Yin Lin,[1] Aleksandr Chernatynskiy,[2] Juan C. Nino,[1] Jacob L. Jones,[3] Richard Hennig,[1] and Susan B. Sinnott[4,a)]
[1]*Department of Materials Science and Engineering, University of Florida, Gainesville, Florida 32611, USA*
[2]*Department of Physics, Missouri University of Science and Technology, Rolla, Missouri 65409, USA*
[3]*Department of Materials Science and Engineering, North Carolina State University, Raleigh, North Carolina 27695, USA*
[4]*Department of Materials Science and Engineering, Pennsylvania State University, University Park, Pennsylvania 16801, USA*

(Received 29 April 2016; accepted 5 July 2016; published online 29 July 2016)

The formation of intermetallic secondary phases, such as Pt_3Pb, has been observed experimentally at $PbTiO_3$/Pt and $Pb(Zr,Ti)O_3$/Pt, or PZT/Pt, interfaces. Density functional theory calculations are used here to calculate the work of adhesion of these interfacial systems with and without the secondary intermetallic phase. The charge density maps of the interfaces reveal the electronic interactions at the interface and the impact of the secondary phase. In addition, Bader charge analysis provides a quantitative assessment of electron transfer from the perovskites to the Pt. Analysis of the band diagrams indicates an increase of the potential barrier associated with electron transfer due to the formation of the Pt_3Pb at PZT/Pt interfaces. *Published by AIP Publishing.* [http://dx.doi.org/10.1063/1.4959074]

I. INTRODUCTION

Perovskite oxide materials of the form ABO_3 are widely used in many electronic devices. These functional oxides, such as barium titanate ($BaTiO_3$), strontium titanate ($SrTiO_3$), lead titanate (PTO), and lead zirconate titanate (PZT), are designed to function in contact with a metal electrode. Consequently, the heterogeneous interface between the metal and functional oxide plays a crucial role in controlling the performance and durability of the devices in which they are used, including actuators, transducers, and supercapacitors.[1–3] Given the importance of these heterogeneous interfaces, multiple applied[4,5] and fundamental[2,3,6] studies have focused on characterizing and optimizing their properties. This prior work has revealed that such factors as lattice mismatch, composition, and defects have a substantial influence on interfacial properties.

Two systems of particular interest consist of a Pt electrode in contact with PTO or PZT.[7,8] One secondary phase in particular, Pt_3Pb, has been identified at the PZT/Pt interface.[9–11] It has been experimentally shown that the formation of this phase can be minimized by controlling the thermal and atmospheric conditions under which the PZT is grown on the Pt electrode.[12–14] In addition, a combined computational and experimental investigation[15] revealed that the secondary phase forms via Pb diffusion across the interface, a process that can take place over time during the processing of the device.

Here, we use first principles calculations to quantify the way in which the secondary phase influences the work of adhesion and electronic interaction of the atoms near the interfaces for both PTO/Pt and PZT/Pt interfaces. In addition, charge transfer across the interfaces and the predicted band diagrams are considered to investigate the sensitivity of the electronic properties results on the existence of Pt_3Pb at the PZT/Pt interface.

II. COMPUTATIONAL METHODS

The density-functional theory (DFT) calculations are carried out with the local density approximation (LDA) as implemented in the Vienna *Ab initio* Simulation Package (VASP).[16–18] The ion-electron interactions between the core electrons and the nuclei are described by the projector augmented-wave (PAW) method. Instead of using the rapid oscillated wavefunctions from the valence electrons, this approach addresses the wavefunctions from the core electrons more smoothly in order to increase the computational efficiency. A plane-wave cut-off energy of 400 eV and a $4\times4\times1$ k-point mesh ensure that the calculated energies are accurate to within 0.5 meV/atom. The reason we select the LDA instead of the generalized gradient approximation (GGA) is the better agreement of the LDA with experimental values for the lattice parameters of PTO. In particular, LDA predicts a unit cell volume of 59.879 $Å^3$ and a c/a ratio of 1.032, which compares better with the experimental value of 1.063 than that of 1.161 predicted from GGA. Similarly, in the case of the PZT, LDA predicts the c/a ratio of 1.023 which compares well with the experimental value of 1.024.

In the case of the PTO/metal interfaces, the (111) interfaces of both PTO and the Pt electrode are formed by combining two slabs: a PTO slab and either a Pt_3Pb or a Pt slab. The PTO (111)-oriented slabs are built based on the primitive perovskite unit cell which was represented using a hexagonal unit cell with 10 atomic layers perpendicular to the interface. Similarly, the metal slabs are based on the primitive FCC unit cell which was represented using a hexagonal

a)Author to whom correspondence should be addressed. Electronic mail: sinnott@matse.psu.edu

supercell 10 atomic layers perpendicular to the interface. A reference from the literature[19] and our convergence tests indicate that vacuum separations of about 20–26 Å are appropriate for the PTO and metallic slabs. As indicated in Figure 1, the hexagonal unit cell of the PTO perovskite (111) surface has the same structure and energetic presentation as the tetragonal (001) perovskite unit cell. The energy difference between each unit cell for both of these relaxed systems was calculated and the results, provided in Table I, indicate an energy difference of 0.04% that is small enough for us to ignore.

We construct the interface by combining the hexagonal supercells of PTO and the metallic slab. The interfacial strain as a result of lattice mismatch is +3.18% for PTO/Pt_3Pb and −3.19% for PTO/Pt interfaces, and the strain is accommodated on the metallic side of the interface. Two different terminations of PTO (111), Ti- and (Pb, O)-terminated, are indicated in Figures 2(a)–2(d). It is known that PTO undergoes a phase transition from the tetragonal phase to the cubic phase when the system temperature increases above the Curie temperature of 400 °C. Therefore, interfaces with two different c/a ratios of 1.06 and 1.00 were considered in the calculations. The lowest energy configurations of PZT(50/50) structures with different terminations were determined by a substitution test, in which the different Ti atom sites were occupied by Zr atoms in both ordered and random configurations while maintaining the Ti:Zr ratio at 0.5. The details of the PZT/metal interfaces are the same as in Ref. 14, and these interfaces are illustrated in Figure 3.

A multi-step relaxation method was applied to all the interfacial systems to reduce the computational cost. First, the volume and the shape of the supercell were fixed and the atoms were fully relaxed within the cell using a reduced *k*-point mesh of 2×2×1. Second, a denser k-point mesh of 4×4×1 was applied and the atoms were fully relaxed. Third, considering the distance between the slabs in the direction normal to the interface, the metal slabs were manually moved around the x-y plane of the interface and the structures were further relaxed again to have the most energetically stable structure of the system to be chosen. The results indicate that the lowest energy structures occur when the atoms at the top of the Pt_3Pb slabs are shifted 0.5 of a unit cell along the $[\bar{1}\bar{1}2]$ and $[10\bar{1}]$ directions, respectively,

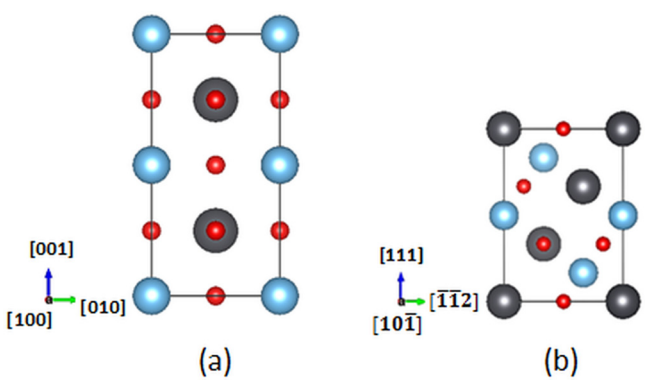

FIG. 1. The transformation of the (a) general perovskite (001) surface unit cells to (b) the primitive perovskite (111) surface unit cells.

TABLE I. Comparison of the total energy of PTO unit cell adapted into tetragonal and hexagonal supercells.

	Total energy (eV/atom)	Difference
In tetragonal cell	−8.385	
In hexagonal cell	−8.382	0.04%

relative to the atoms at the bottom of the PTO slabs within the plane of the interface. In the case of systems with Pt on top of PTO slabs, the lowest energy was found when the shift between the top and bottom slabs is 0.25 of a unit cell length along both $[\bar{1}\bar{1}2]$ and $[10\bar{1}]$ directions within the plane of the interface. Thus, a total of twenty interfacial structures are considered in this work, including eight PTO/metallic and twelve PZT/metallic interfaces.

Once the lowest energy structure of each interface is obtained, the work of adhesion is determined. In addition, contour plots of the electronic density maps are generated using VISTA software[20,21] to describe the electronic interaction between atoms at the interface. Bader charge analysis[22,23] is also used to provide a quantitative assessment of charge transfer across the interface. In this way, the total amount of charge transferred across the interfaces that results in the difference of electronegativity between adjacent atoms associated to the induced polarization can be obtained.

Band diagrams of different contacts are analyzed to elucidate the impact of the secondary phase on the charge transfer once contact is made. The electrostatic potentials are determined for the metallic and perovskite slabs that are separated with a sufficient vacuum space to obtain the work function of either the Pt or the Pt_3Pb slabs and the valence band of the PZT slab. In particular, the electrostatic potentials of the metal and perovskite are aligned along the vacuum level to create the energy band diagrams for the different

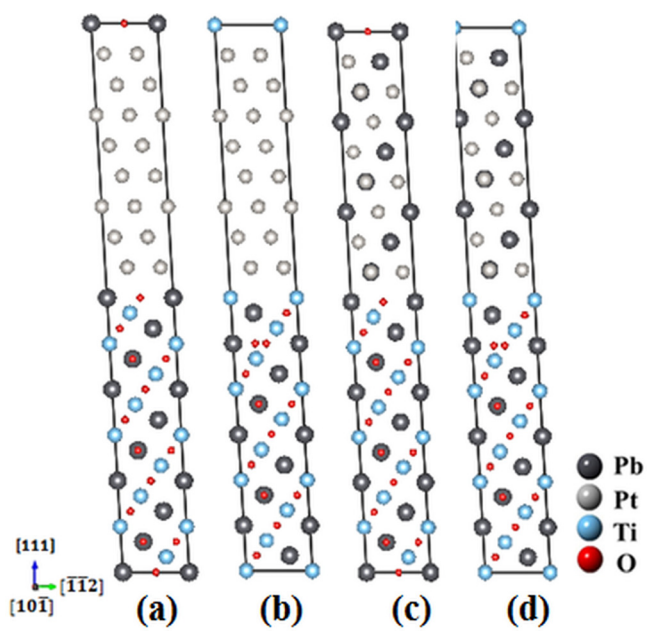

FIG. 2. Illustrations of the supercells used in the DFT calculations for the (a) (Pb,O)-terminated PTO/Pt interface, (b) Ti -terminated PTO/Pt interface, (c) (Pb,O)-terminated PTO/Pt_3Pb interface, and (d) Ti-terminated PTO/Pt_3Pb interfaces.

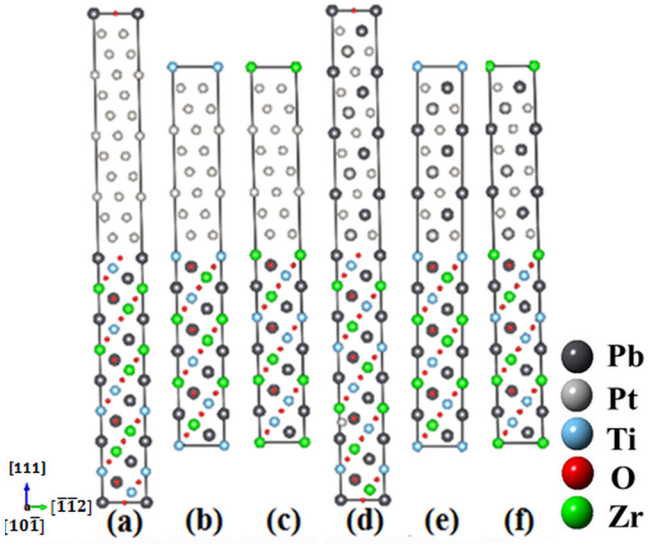

FIG. 3. Illustrations of the supercells used in the DFT calculations for the (a) (Pb,O)-terminated PZT/Pt interface, (b) Ti-terminated PZT/Pt interface, (c) Zr-terminated PZT/Pt interface, (d) (Pb,O)-terminated PZT/Pt_3Pb interface, and (e) Ti-terminated PZT/Pt_3Pb interface and (f) Ti-terminated PZT/Pt_3Pb interfaces.

interfaces. The band gap of PZT was predicted by the band diagram and projected density of states (PDOS) using LDA with 10 k-points along the most symmetric direction of the first Brillouin zone. As LDA is known to underestimate the band gap of perovskite, a more accurate band gap energy between the conduction band and the valence band of PZT was calculated using the HSE06 hybrid functional.[24–26] The projected density of state (PDOS) at the gamma point was carried out by hybrid functional calculation as a correction for the underestimated band gap of PZT from the DFT-LDA calculations.

III. RESULTS AND DISCUSSION

A. Interfacial work of adhesion and structure

The work of adhesion is calculated using the standard expression

$$\text{Work of Adhesion Energy (WOA)} = \frac{1}{2A}\left((E_{surface\,1} + E_{surface\,2}) - E_{interface}\right). \quad (1)$$

The quantitative values of WOA and the corresponding interfacial structures are provided in Figure 3 for PTO/metal interfaces. At low temperatures, the PTO/Pt interfaces have a work of adhesion of 0.165 eV/Å^2 for (Pb,O)-terminated and 0.178 eV/Å^2 for Ti-terminated interfaces. These values are higher than the corresponding PTO/Pt_3Pb interfaces: 0.151 eV/Å^2 for (Pb,O)-terminated and 0.156 eV/Å^2 for Ti-terminated interfaces. Thus, the PTO/Pt interfaces are more energetically favorable than the PTO/Pt_3Pb interfaces.

A similar trend of work of adhesion for each corresponding interface is predicted for the high temperature phase PTO-related interfaces. The PTO/Pt interfaces again have higher work of adhesion than PTO/Pt_3Pb interfaces. However, the work of adhesion for PTO/Pt_3Pb in the high temperature phase of PTO is smaller than in the low temperature phase due to the much larger lattice mismatch (+7.56%) for the cubic-PTO/Pt_3Pb interfaces. In contrast, the work of adhesion for cubic-PTO/Pt interfaces is larger than in the low temperature phase PTO system because of the smaller lattice mismatch (+0.92%) for cubic-PTO/Pt.

The results indicate that the Ti-terminated interfaces generally have larger WOA values than (Pb, O)-terminated interfaces. In addition, PTO/Pt interfaces are more energetically favorable than the PTO/Pt_3Pb. The results further indicate the way in which lattice mismatch is crucial for the work of adhesion at these interfaces.

The quantitative values and a similar trend for WOA are found for PZT-related interfaces as summarized in Figure 4. Compared with the PTO systems, the PZT models include additional Zr-terminated interfaces. However, this termination is not predicted to be preferred (Fig. 5). Thus, composition of the perovskite does not have a substantial impact on the close-packed interfacial work of adhesion.

Atomic displacement across the various interfaces considered is illustrated in Figure 6. Surface Ti atoms relax inward (toward bulk PTO bulk) at the Ti-terminated PTO/Pt interface. Interfacial Ti atoms exhibit more displacement toward bulk PTO at the PTO/Pt_3Pb interface compared with the PTO/Pt interface. In the (Pb, O)-terminated PTO/Pt interface, relaxation is more nuanced. Namely, surface Pb atoms relax inward (toward PTO bulk) while O atoms relax outward (away from PTO bulk). Moreover, surface O atoms adjacent to Pt from Pt_3Pb are displaced away from bulk PTO but those adjacent to Pb atoms from the Pt_3Pb phase are

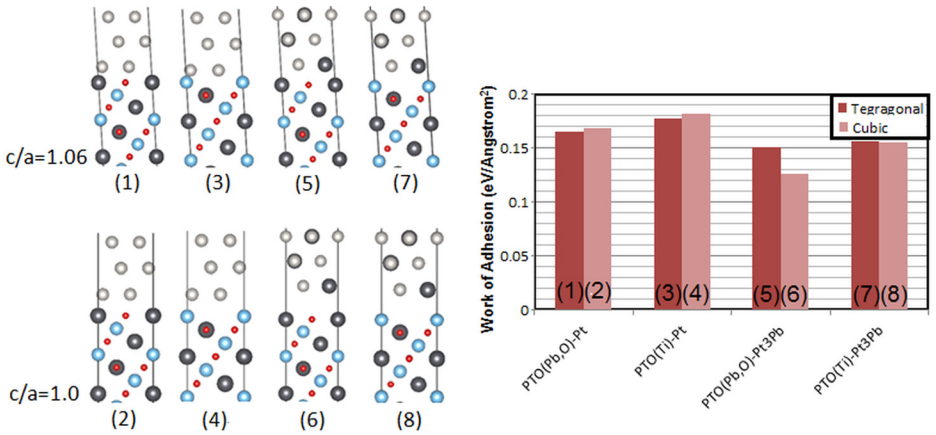

FIG. 4. The quantitative values of WOA and the corresponding interfacial structures for PTO/metal or alloy interfaces, where we predict (1) 0.165 (eV/Å^2) for the t-PTO(Pb,O) /Pt interface, (2) 0.169 (eV/Å^2) for the c-PTO(Pb,O)/Pt interface, (3) 0.178 (eV/Å^2) for the t-PTO(Ti)/Pt interface, (4) 0.182 (eV/Å^2) for the c-PTO(Ti)/Pt interface, (5) 0.151 (eV/Å^2) for the t-PTO(Pb,O) /Pt_3Pb interface, (6) 0.126 (eV/Å^2) for the c-PTO(Pb,O) /Pt_3Pb interface, (7) 0.156 (eV/Å^2) for the t-PTO(Ti) /Pt_3Pb interface, and (8) 0.155 (eV/Å^2) for the c-PTO(Ti) / Pt_3Pb interface.

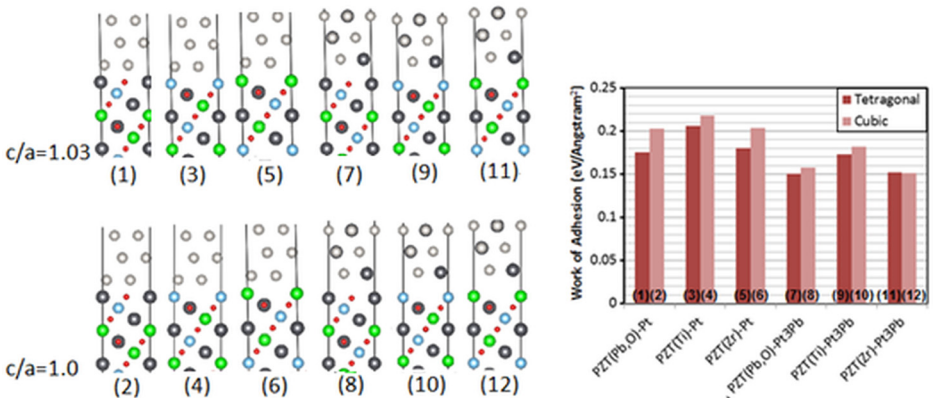

FIG. 5. The quantitative values of WOA and the corresponding interfacial structures for PZT/metal or alloy interfaces, where we found (1) 0.175 (eV/Å^2) for the t-PZT(Pb,O)/Pt interface, (2) 0.234 (eV/Å^2) for the c-PZT(Pb,O)/Pt interface, (3) 0.206 (eV/Å^2) for the t-PZT(Ti)/Pt interface, (4) 0.218 (eV/Å^2) for the c-PZT(Ti)/Pt interface, (5) 0.180 (eV/Å^2) for the t-PZT(Zr)/Pt interface, (6) 0.204 (eV/Å^2) for the c-PZT(Zr)/Pt interface, (7) 0.150 (eV/Å^2) for the t-PZT(Pb,O) /Pt_3Pb interface, (8) 0.149 (eV/Å^2) for the c-PZT(Pb,O) /Pt_3Pb interface, (9) 0.173 (eV/Å^2) for the t-PZT(Ti) /Pt_3Pb interface, (10) 0.183 (eV/Å^2) for the c-PZT(Ti) /Pt_3Pb interface, (11) 0.151 (eV/Å^2) for the t-PZT(Zr) /Pt_3Pb interface, and (12) 0.160 (eV/Å^2) for the c-PZT(Zr) /Pt_3Pb interface.

displaced toward PTO. This difference indicates stronger interaction between O of the perovskite phase and the Pt atoms in the Pt_3Pb phase than the Pb atoms in the Pt_3Pb phase.

Very similar results were found for the (Pb,O)- and Ti-terminated PZT/Pt and PZT/Pt_3Pb interactions. The additional Zr-terminated system illustrated in Figure 7 behaves in a similar manner as the Ti-terminated system. This indicates that for these systems, changes in the perovskite composition between PTO and PZT do not have a substantial effect on the interfacial stability.

B. Interfacial electronic structure

The charge density maps of PTO interfaces had been discussed by us previously,[15] and our findings are consistent with Stengel and Spaldin's result in Ref. 27. In particular, their findings indicate that strong interactions exist between Pt and O atoms at both the (Pt, O)-terminated PTO/Pt and PTO/Pt_3Pb interfaces and they concluded that the PTO/Pt interface is energetically preferred.

A similar conclusion regarding interfacial charge density is shown in Figures 8(a)–8(f) for PZT interfaces with various terminations. In particular, the electronic density maps indicate that a similar strong interaction exists between the Pt atoms of the metal slab and Pb or O atoms in the PZT slabs for these three types of terminated PZT/Pt interfaces. The visualized high charge density areas in the map directly illustrate the prediction that the attractive interaction between Pt and O is much stronger than that between the Pb

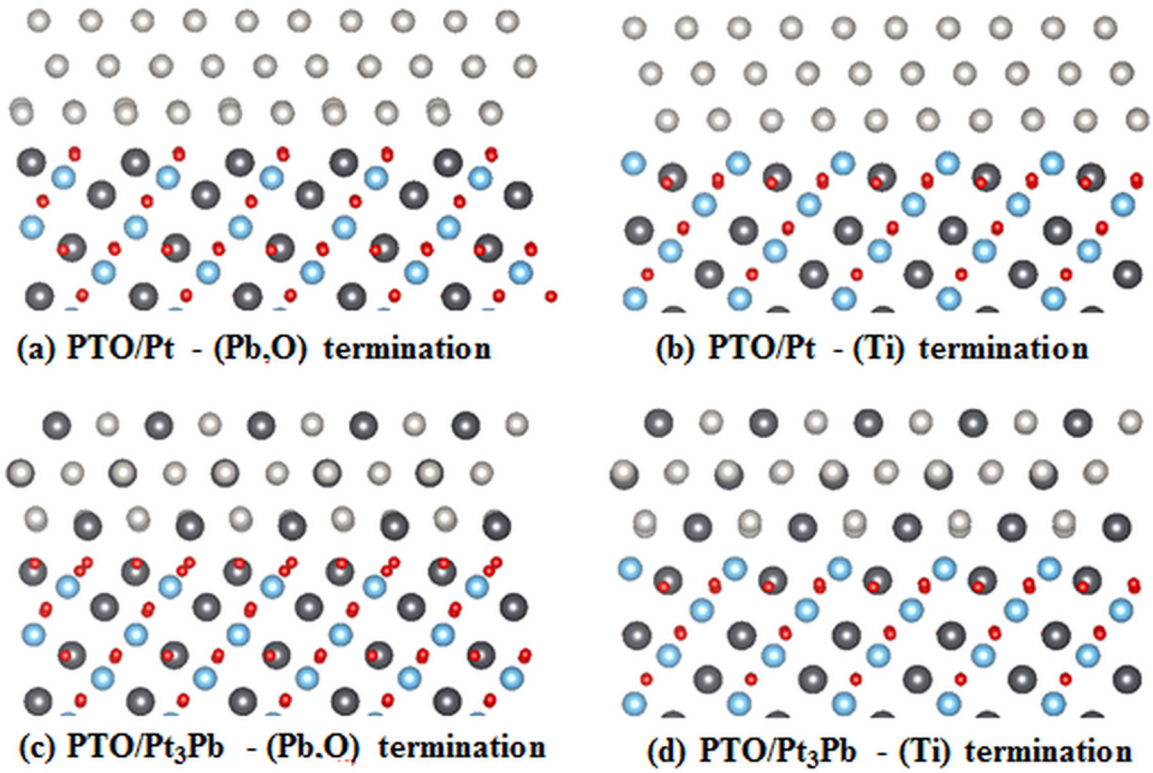

FIG. 6. The interfaces images of PTO/Pt and PTO/Pt_3Pb interfaces with different PTO terminations.

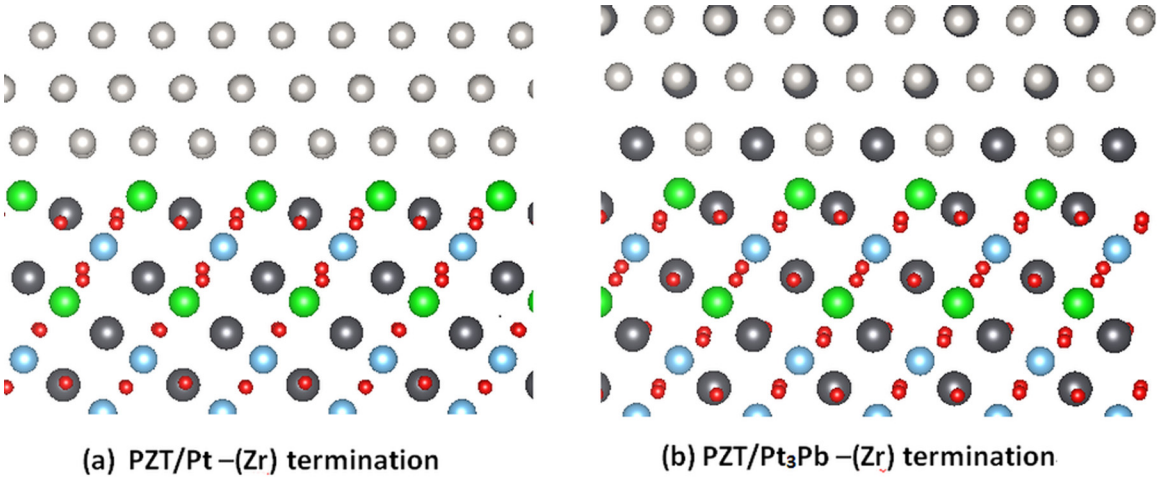

FIG. 7. The interfaces images of (a) PZT/Pt and (b) PZT/Pt_3Pb interfaces with Zr- termination.

and O atoms and that the former forms a true chemical bond. More Pt atoms are present in the contact layer for the PZT/Pt system than for the PZT/Pt_3Pb system, which contributes to the increased stability of the PZT/Pt interface. The electronic density maps of Zr-terminated and Ti-terminated interfaces in Figures 8(c)–8(f) are comparable, where Zr behave like the Ti atoms. This result further supports the hypothesis that the substituted Zr atoms in perovskite PZT and PTO structures do not have a substantial effect on electronic structure.

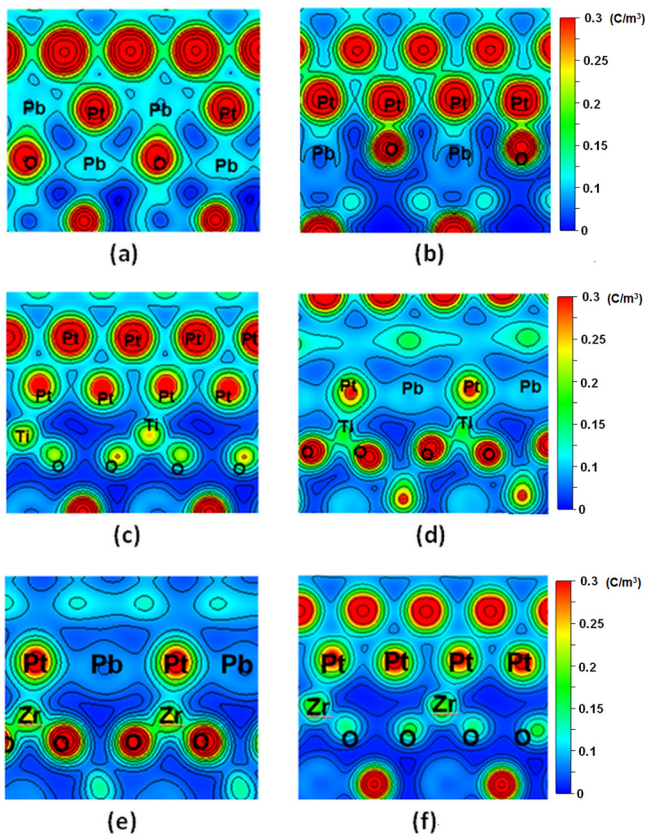

FIG. 8. The charge density maps of three types of differently terminated PZT/Pt_3Pb and PZT/Pt interfaces. (a) PZT/Pt with (Pb,O)-termination, (b) PZT/Pt_3Pb with (Pb,O)-termination, (c) PZT/Pt with Ti-termination, (d) PZT/Pt_3Pb with Ti-termination, (e) PZT/Pt with Zr-termination, and (f) PZT/Pt_3Pb with Zr-termination.

Additionally, Figure 9 shows three cross sectional charge density images of the Ti-terminated PTO/Pt system. Figure 9(a) indicates that the Ti atoms are not in the same plane as the Pb, Pt, and O atoms in this cross section image of interface, so no interaction between the contact layer of Pt and Ti is expected. However, the Ti atoms still have some interaction with surface O atoms from PTO, as shown in Figure 9(b). Figure 9(c) confirms that the Pt, Pb, and O atoms lie on the same plane and the stronger interaction takes place between Pt and O rather than Pt and Pb.

The following discussion of electronic properties focuses on the PZT related interfaces since they are more favorable for current manufacturing. The electronic charge transfer at the interface is quantified using Bader charge calculations. Figures 10 and 11 represent Bader charge differences as a function of the axis normal to the interface for atoms at the PZT/Pt_3Pb (Figure 10) and PZT/Pt (Figure 11) interfaces. The results reveal that charge transfer primarily takes place in the interfacial region. Since the models are periodic along the direction normal to the interface, the interfaces in these two figures can be identified at three points that

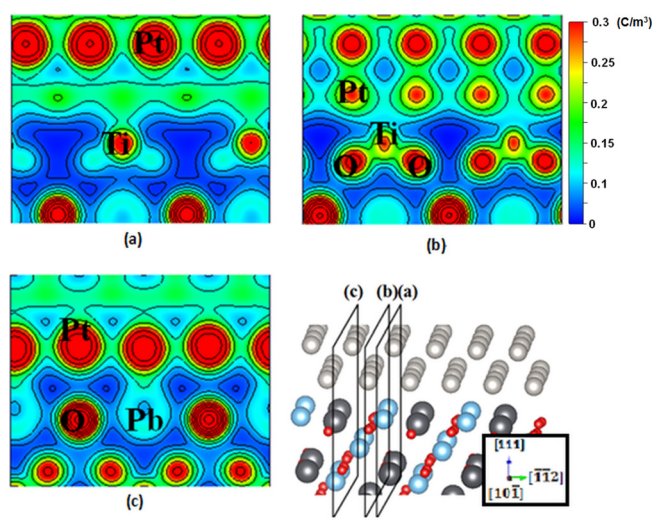

FIG. 9. The charge density maps of Ti terminated PTO/Pt interface in different cross-sections.

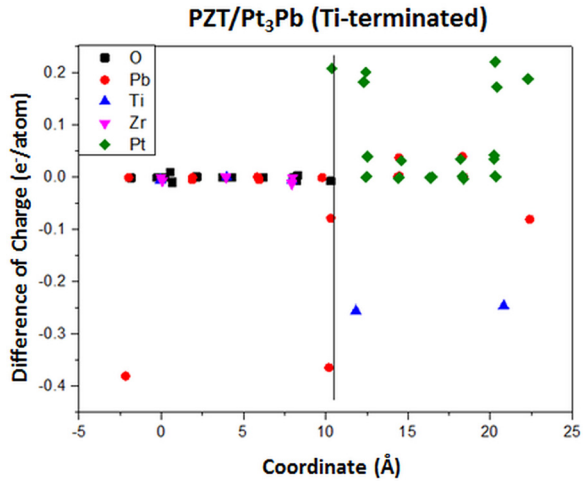

FIG. 10. The representative of charge transfer per atom in the Ti terminated PZT/Pt3Pb interface as function as Z coordinate.

correspond to z-coordinate = −2.5 Å, 10.0 Å, and 22.5 Å, respectively. (Note, the PZT/Pt or PZT/Pt_3Pb interfaces are at 0 Å.) A significant electronic screening phenomenon, in particular, at the Pt slab, can be found at the interfaces and causes the formation of the effective dead layer which can reduce the interfacial capacitance.[27,28] However, Stengel and Spaldin reported that the PTO/Pt system has relative short screening length so that it becomes negligible and we only consider the atoms near the interfaces. The atoms located around these three interfacial regions undergo a significantly larger change in Bader charge than do those atoms located in the middle of the slabs from either gaining or losing electrons.

Not surprisingly, different types of atoms gain or lose electrons in different ways, a phenomenon which also depends on the material itself and the atom's surrounding environment. In this particular material, Pb, Ti, and O lose electrons where the PZT contacts the Pt surface and the Pt atoms are likely to gain electrons. A screening of electrons can also be found in the first two atomic layers near the interfaces. The charge transfer of Pb atoms depends substantially

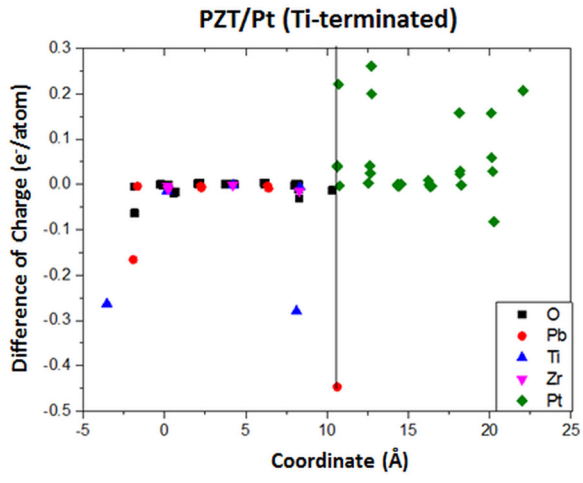

FIG. 11. The representative of charge transfer per atom in the Ti terminated PZT/Pt interface as function as Z coordinate.

TABLE II. The quantitative assessment of charge changes for those atoms which are close to the Ti terminated PZT-Pt_3Pb and PZT-Pt interfaces. (Pt* is the atoms substituted by Pb once in the Pt_3Pb slab).

	PZT-Pt_3Pb-(Ti-termination)		PZT-Pt-(Ti-termination)	
Interfaces	Atom type	Δq	Atom type	Δq
	Pb	−0.078	Pt*	−0.003
	Pt	0.183	Pt	0.261
	Pt	0.202	Pt	0.221
Pt3Pb/Pt side	Pt	0.209	Pt	0.2
	Pb	−0.365	Pb	−0.447
	Ti	−0.256	Ti	−0.279
	O	−0.007	O	−0.031
	O	0.003	O	−0.012
	O	−0.007	O	−0.013
PZT side	Zr	−0.012	Zr	−0.015

on the surrounding environment. It could act as a donor to give away electrons while in the PZT slab and also work like an acceptor to receive electrons when it is part of the metallic (Pt_3Pb) slab. The total quantity of charge transfer cross the interfaces in the PZT/Pt case is larger than in the PZT/Pt_3Pb case (1.4 electrons vs. 0.8 electrons, respectively). A larger charge transfer indicates a stronger interaction between two slabs and thus a more stable interface. This result is consistent with our WOA calculation results that predict the PZT/Pt interface to be more favorable.

In addition, the quantitative assessment of charge transfer for each atom is listed in Table II to clarify the charge transfer contribution. Comparing the electron acceptance of the Pt atoms located in the first atomic layer for both PZT/Pt and PZT/Pt_3Pb interfaces, Pt atoms in the Pt slab receive more electrons than those in the Pt_3Pb slab. On the other hand, comparing the electron donation of the atoms located in the first atomic layer of the PZT slab, the Pb, Ti, O, and Zr, atoms in the PZT/Pt interfaces also lose more electrons than those in the PZT/Pt_3Pb interface. The larger the difference in electronegativity for adjacent atoms on either side of the interface, the more charge transfer takes place at the PZT/Pt interface. This leads to the formation of stronger ionic bonds and a more energetically favorable interface.

C. Influence of secondary phase on electronic contact

To understand the influence of the formation of the secondary phase Pt_3Pb on the contact between PZT and Pt, the band diagrams of Pt, Pt_3Pb, and PZT slabs are combined, as illustrated in Figures 12 and 13. After aligning the electrostatic potentials relative to the vacuum level, the work function of Pt and Pt_3Pb are determined to be −6.02 eV and −5.06 eV, respectively, and the valence band maximum of PZT is −7.47 eV. We utilized the band structure and projected density of states (PDOS) from the LDA calculations that underestimate the true band gap. Hybrid functional calculations are then applied to determine a more accurate, corrected band gap by taking into account the difference of the projected density states results between the LDA and hybrid functional. The corrected band gap of PZT using the combination of LDA and

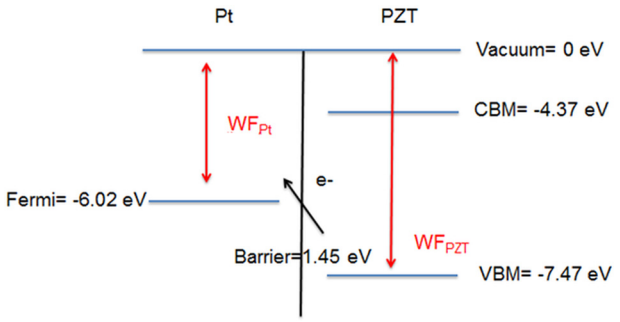

FIG. 12. The prediction of band diagram on PZT/Pt contact.

hybrid functionals is 3.1 eV which is within the experimentally measured range of 3.0 eV−3.7 eV.[29–31] In particular, we found that the PZT slabs with different terminations create extra interval energy levels in the band diagrams when compared with the normal band gap diagram obtained from bulk PZT. It should be noted that we exclude the extra interval energy levels resulting from artificially adding terminated atoms to avoid non-stoichiometric effects so that the correct band gap value of PZT can be used to determine electronic band diagrams for contacts between PZT and metallic layers (Pt or Pt_3Pb). This result, shown in Figures 12 and 13, predict that a higher energy barrier exists in PZT/Pt_3Pb than in PZT/Pt. Published results[32,33] indicate that the electrons transferred from the PZT slab into the Pt_3Pb slab needs to overcome a higher potential barrier than electrons transferred into the Pt slab. Thus, more electrons transfer and there is a stronger induced interface dipole at the PZT/Pt interface. This prediction thus provides guidance for experimentalists to understand the way in which energy barriers that need to be overcome during the transportation of holes and electrons at the interfaces of perovskite and metallic layers and the electronic behaviors of the devices.

IV. CONCLUSIONS

We use first principles calculations to examine both interfacial stability and the electronic properties across the interfaces coming from the formation of secondary phase at the perovskite and metal contact, especially PZT/Pt in this present work.

The work of adhesion result examines how the formation of the Pt_3Pb intermetallic layers reduces the interfacial stability of the metal/perovskite interfaces in both PTO and PZT related interfaces and further proven by the electronic density calculation and the Bader charge analysis. The different ratio for the Zr and Ti substitution does not cause a substantial effect on the electronic interaction in the interfaces. A higher energy barrier is predicted to exist when Pt_3Pb forms at the PZT/Pt contact which eliminates the interfacial dipole and electron charge transfer in electronic devices. Therefore, the existence of the secondary phase in this particular material system is considered to have a negative impact on thermal stability and increase the potential barrier at the perovskite/metal contact. Furthermore, the approaches we present in this work can be a useful tool for identifying the impacts secondary phase made in various material properties for metal and perovskite contacts.

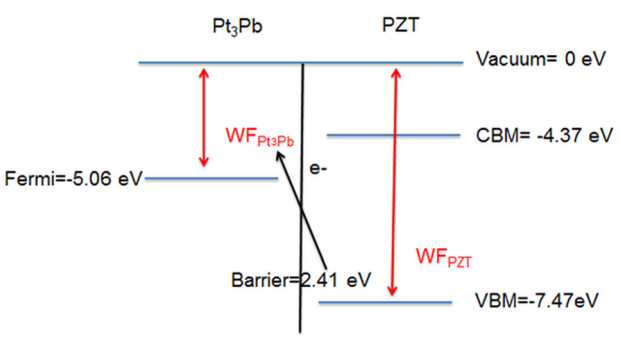

FIG. 13. The prediction of band diagram on PZT/Pt_3Pb contact.

ACKNOWLEDGMENTS

The authors acknowledge support for this work under NSF Award No. DMR-1207293 and the use of the High-Performance Computing (HPC) at the University of Florida, which is supported by the UF Research Computing Center.

[1]S. Saadon and O. Sidek, "A review of vibration-based MEMS piezoelectric energy harvesters," Energy Convers. Manage. **52**(1), 500–504 (2011).
[2]N. Setter, D. Damjanovic, L. Eng, G. Fox, S. Gevorgian, S. Hong, A. Kingon, H. Kohlstedt, N. Y. Park, G. B. Stephenson, I. Stolitchnov, A. K. Taganstev, D. V. Taylor, T. Yamada, and S. Streiffer, "Ferroelectric thin films: Review of materials, properties, and applications," J. Appl. Phys. **100**(5), 051606 (2006).
[3]D. I. Woodward, J. Knudsen, and I. M. Reaney, "Review of crystal and domain structures in the $PbZr_xTi_{1-x}O_3$ solid solution," Phys. Rev. B **72**(10), 104110 (2005).
[4]S. I. Hirano, T. Yogo, K. Kikuta, Y. Araki, M. Saitoh, and S. Ogasahara, "Synthesis of highly oriented lead zirconate–lead titanate film using metallo-organics," J. Am. Ceram. Soc. **75**(10), 2785–2789 (1992).
[5]M. T. Kesim, J. Zhang, S. Trolier-McKinstry, J. V. Mantese, R. W. Whatmore, and S. P. Alpay, "Pyroelectric response of lead zirconate titanate thin films on silicon: Effect of thermal stresses," J. Appl. Phys. **114**(20), 204101 (2013).
[6]S.-Y. Chen and I. W. Chen, "Texture development, microstructure evolution, and crystallization of chemically derived PZT thin films," J. Am. Ceram. Soc. **81**(1), 97–105 (1998).
[7]S.-Y. Chen and I. W. Chen, "Temperature–time texture transition of Pb(Zr1−xTix)O_3 thin films: I, Role of Pb-rich intermediate phases," J. Am. Ceram. Soc. **77**(9) 2332–2336 (1994).
[8]Z. Zhang, P. Wu, L. Lu, and C. Shu, "*Ab initio* study of formations of neutral vacancies in ferroelectric $PbTiO_3$ at different oxygen atmospheres," J. Alloys Compd. **449**(1–2), 362–365 (2008).
[9]Z. Huang, Q. Zhang, and R. Whatmore, "The role of an intermetallic phase on the crystallization of lead zirconate titanate in sol–gel process," J. Mater. Sci. Lett. **17**(14), 1157–1159 (1998).
[10]Z. Huang, Q. Zhang, and R. W. Whatmore, "Low temperature crystallization of lead zirconate titanate thin films by a sol-gel method," J. Appl. Phys. **85**(10), 7355–7361 (1999).
[11]K. Nittala, S. Mhin, K. M. Dunnigan, D. S. Robinson, J. F. Ihlefeld, P. G. Kotula, G. L. Brennecka, and J. L. Jones, "Phase and texture evolution in solution deposited lead zirconate titanate thin films: Formation and role of the Pt_3Pb intermetallic phase," J. Appl. Phys. **113**(24), 244101 (2013).
[12]S. Mhin, C. Cozzan, K. Nittala, P. Wanninkhof, J. F. Ihlefeld, G. L. Brennecka, and J. L. Jones, "Effect of switching atmospheric conditions during crystallization on the phase evolution of solution-derived lead zirconate titanate thin films," J. Am. Ceram. Soc. **96**(9), 2706–2709 (2013).
[13]K. Tokita, M. Aratani, and H. Funakubo, "Effect of atmosphere during heating of substrate on the low temperature deposition of metalorganic chemical vapor deposited $Pb(Zr_x,Ti_{1-x})O_3$ thin films," Appl. Phys. Lett. **81**(5), 898–900 (2002).
[14]F.-Y. Lin, A. Chernatynskiy, J. Nikkel, R. Bulanadi, J. L. Jones, J. C. Nino, and S. B. Sinnott, "Diffusion across M/Pb(Zr,Ti)O_3 interfaces

($M = Pt_3Pb$ or Pt) under different system conditions," J. Am. Ceram. Soc. **99**(1), 356–362 (2015).
[15]J. L. Jones, J. M. LeBeau, J. Nikkel, A. Oni, H. Dycus, C. Cozzan, F.-Y. Lin, A. Chernatynskiy, J. C. Nino, S. B. Sinnott, S. Mhin, G. L. Brennecka, and J. Ihlefeld, "Combined experimental and computational methods reveal the evolution of buried interfaces during synthesis of ferroelectric thin films," Adv. Mater. Interfaces **2**(10), 1500181 (2015).
[16]G. Kresse and J. Furthmüller, "Efficiency of *ab-initio* total energy calculations for metals and semiconductors using a plane-wave basis set," Comput. Mater. Sci. **6**(1), 15–50 (1996).
[17]J. Hafner, "Materials simulations using VASP—A quantum perspective to materials science," Comput. Phys. Commun. **177**(1–2), 6–13 (2007).
[18]R. A. Evarestov, A. I. Panin, A. V. Bandura, and M. V. Losev, "Electronic structure of crystalline uranium nitrides UN, U 2 N 3 and UN 2: LCAO calculations with the basis set optimization," J. Phys.: Conf. Ser. **117**(1), 012015 (2008).
[19]A. M. Kolpak, N. Sai, and A. M. Rappe, "Short-circuit boundary conditions in ferroelectric $PbTiO_3$ thin films," Phys. Rev. B **74**(5), 054112 (2006).
[20]K. A. Frazer, L. Pachter, A. Poliakov, E. M. Rubin, and I. Dubchak, "VISTA: Computational tools for comparative genomics," Nucl. Acids Res. **32**(suppl 2), W273–W79 (2004).
[21]C. Mayor, M. Brudno, J. R. Schwartz, A. Poliakov, E. M. Rubin, K. A. Frazer, L. S. Pachter, and I. Dubchak, "VISTA: Visualizing global DNA sequence alignments of arbitrary length," Bioinformatics **16**(11), 1046–1047 (2000).
[22]G. Henkelman, A. Arnaldsson, and H. Jónsson, "A fast and robust algorithm for Bader decomposition of charge density," Comput. Mater. Sci. **36**(3), 354–360 (2006).
[23]W. Tang, E. Sanville, and G. Henkelman, "A grid-based Bader analysis algorithm without lattice bias," J. Phys.: Condens. Matter **21**(8), 084204 (2009).
[24]J. Paier, M. Marsman, K. Hummer, G. Kresse, I. C. Gerber, and J. G. Ángyán, "Screened hybrid density functionals applied to solids," J. Chem. Phys. **124**(15), 154709 (2006).
[25]A. V. Krukau, O. A. Vydrov, A. F. Izmaylov, and G. E. Scuseria, "Influence of the exchange screening parameter on the performance of screened hybrid functionals," J. Chem. Phys. **125**(22), 224106 (2006).
[26]S. Piskunov, E. Heifets, R. I. Eglitis, and G. Borstel, "Bulk properties and electronic structure of $SrTiO_3$, $BaTiO_3$, $PbTiO_3$ perovskites: An *ab initio* HF/DFT study," Comput. Mater. Sci. **29**(2), 165–178 (2004).
[27]M. Stengel, D. Vanderbilt, and N. A. Spaldin, "Enhancement of ferroelectricity at metal-oxide interfaces," Nat. Mater. **8**(5), 392–397 (2009).
[28]M. Stengel and N. A. Spaldin, "Origin of the dielectric dead layer in nanoscale capacitors," Nature **443**(7112), 679–682 (2006).
[29]H. Lin, N. J. Wu, F. Geiger, K. Xie, and A. Ignatiev, "Photoresponse and fast optical readout for a $PbZr_xTi_{1-x}O_3/YBa_2Cu_3O_{7-x}$ thin-film heterostructure capacitor," Appl. Phys. Lett. **66**(10), 1172–1174 (1995).
[30]S. K. Pandey, A. R. James, R. Raman, S. N. Chatterjee, A. Goyal, C. Prakash, and T. C. Goel, "Structural, ferroelectric and optical properties of PZT thin films," Physica B: Condens. Matter **369**(1–4), 135–142 (2005).
[31]J. Robertson, C. W. Chen, W. L. Warren, and C. D. Gutleben, "Electronic structure of the ferroelectric layered perovskite $SrBi_2Ta_2O_9$," Appl. Phys. Lett. **69**(12), 1704–1706 (1996).
[32]I. Stolichnov and A. Tagantsev, "Space-charge influenced-injection model for conduction in $Pb(Zr_xTi_{1-x})O_3$ thin films," J. Appl. Phys. **84**(6), 3216–3225 (1998).
[33]D. J. Wouters, G. J. Willems, and H. E. Maes, "Electrical conductivity in ferroelectric thin films," Microelectron. Eng. **29**(1–4), 249–256 (1995).